ISSN 0915-633X

NATIONAL INSTITUTE FOR FUSION SCIENCE

Low-Dimensional Model of Resistive Interchange Convection in Magnetized Plasma

S. Bazdenkov and T. Sato

(Received - Aug. 15, 1997)

NIFS-505 Sep. 1997

This report was prepared as a preprint of work performed as a collaboration reserch of the National Institute for Fusion Science (NIFS) of Japan. This document is intended for infomation only and for future publication in a journal after some rearrangements of its contents.

Inquiries about copyright and reproduction should be addressed to the Research Information Center, National Institute for Fusion Science, Oroshi-cho, Toki-shi, Gifu-ken 509-02 Japan.

RESEARCH REPORT
NIFS Series

NAGOYA, JAPAN

Low-Dimensional Model of Resistive Interchange Convection in Magnetized Plasma

Sergey Bazdenkov and Tetsuya Sato

Theory and Computer Simulation Center, National Institute for Fusion Science
322-6 Oroshi-cho Toki-shi Gifu-ken 509-52, Japan

Abstract

Self-organization and generation of large shear flow component in turbulent resistive interchange convection in magnetized plasma is considered. The effect of plasma density-electrostatic potential coupling via the inertialess electron dynamics along the magnetic field is shown to play significant role in the onset of shear component. The results of large-scale numerical simulation and low-dimensional (reduced) model are presented and compared.
Keywords: plasma transport, turbulent convection, Edge Localized Modes.

1. INTRODUCTION

One of the serious problem in thermonuclear plasma confinement is anomaly of particle and energy transport caused by plasma convection across the magnetic field. This convection is driven by free energy release during the growth of perturbations in generically unstable thermonuclear plasma.

The most dangerous consequences for plasma confinement might arise from the development of magnetic perturbation which can cause rearrangement of magnetic configuration and trigger its complete disruption. For this reason, magnetic configuration and plasma parameters are usually chosen in the way when such a perturbation is as much suppressed as possible. There are many experimental evidences that, indeed, in large tokamaks and stellarators the magnetic perturbations are basically absent, especially in the peripheral plasma near magnetic separatrix and scrape-off-layer (SOL).

In the absence of magnetic perturbation, plasma convection across strong confining magnetic field is mainly controlled by electrostatic field and pressure gradient forces which cause drift vortex flow perpendicular to both the magnetic field and the force. This flow, in turn, leads to self-consistent spatial redistribution of plasma density and electrostatic potential. Within one-turn-over time scale, such a nonlinear vortex flow becomes complicated and is usually treated in terms of drift turbulence. The corresponding turbulent convection is widely believed to be the cause of transport anomaly in magnetized plasma. In such a scenario, the stronger

fluctuations of plasma density and electrostatic potential correspond to higher convective transport, i.e., exactly what is observed in the low-confinement (L) mode in tokamaks and other machines.

In contrast to L-mode, there also exists high-confinement (H) mode of operation when fairly intensive turbulent convection near the separatrix spontaneously undergoes drastic self-reorganization with consequent improvement in plasma confinement. Depending on plasma parameters, the transition from L- to H- regime may occur in reversible way in the form of edge-localized modes (ELMs). In this case, the configuration spontaneously, but repeatedly, returns to L-regime with further transition to H-mode and so on.

A key and universal feature of the improved confinement mode observed in various plasmas in tokamaks (1-6), stellarators (7-10) and linear machine (11) is the generation of radial electric field and poloidal shear flow (here radial direction corresponds to minor radius of toroidal plasma, i.e., the direction of confinement, while the poloidal direction corresponds to minor bypass around magnetic axis). Generation of shear flow is usually accompanied by considerable suppression of plasma density and potential fluctuations, so that the convective turbulent transport is essentially reduced as well. Respectively, a mechanism for self-consistent shear flow generation is a necessary moment in understanding the physics of the observed L-H transition.

Concerning this problem, two different scenarios are usually considered: either i) generation of radial electric field via the process of charged particle orbit loss (i.e., the kinetic effect), or ii) shear flow self-generation via nonlinear interaction and reconnection of the instability-driven convective cells (see (12-14)). The latter seems to be strong candidate because it is based on a robust effect which could be easily treated in terms of drift plasma fluid dynamics. The details of nonlinear interaction of driving instability and self-consistently generated shear flow depend, of course, on the peculiarities of the considered plasma dynamics.

In the case of edge localized modes (ELMs) in the scrape-off layer (SOL) plasma, which is our main concern in the present paper, experimentally observed edge plasma perturbations are usually of a flute-type character, i.e., look like a "dense" or "hot" plasma filament strongly alongated along the magnetic field (see, e.g., (15,16)). They are localized at the outside of the torus and exist even in the case when pressure gradient near the edge plasma is well below the ideal ballooning stability threshold (hence, no considerble magnetic perturbation is developed). Such a features indicate that driving instability in the SOL is, probably, a kind of pressure-driven resistive interchange (RI) mode akin to a flute-like mode in open systems (this is because of a lack of closed magnetic surfaces in the SOL). Interchange instability is also akin to Rayleigh-Taylor instability in stratified fluid, so that one can expect the onset of Bénard-like convection at the nonlinear stage of interchange instability. Indeed, proposed in (17) and also considered in (18-22), the model of self-consistent generation of Bénard-like convective cells with their periodic rearrangement into the shear flow at the nonlinear stage of RI-instability reproduces qualitatively well many important features of the ELMs.

In the present paper we consider further development of this model mainly in the part concerning the effect of plasma density - electrostatic potential coupling, i.e., a tendency to establish Boltzman distribution, which arises as a result

of dynamical force balance for inertialess electrons in the presence of pressure and potential inhomogeneouty along the field lines. This is a well-known effect which plays important role. for example, in drift plasma dynamics based on Hasegawa-Mima equation. The point, however, is that the Boltzman coupling is usually considered for the poloidally periodical perturbations only. I.e, only the deviations of plasma density and potential from their poloidally averaged background profiles are assumed to be inhomogeneous along the magnetic field and, hence, coupled via electron longitudinal dynamics. At the same time, poloidally averaged background profiles, as themselves, are supposed to be longitudinally homogeneous. In the bulk plasma with closed magnetic surfaces this assumption is quite reasonable because the poloidal averaging, in this case, corresponds simultaneously to the averaging along magnetic field line. But in the case of SOL plasma with open magnetic field lines the procedure of poloidal averaging does not necessarily correspond to the averaging along the field line, and the background pressure and potential profiles are not necessarily homogeneous along the magnetic field. In the toroidal SOL plasma such a longitudinal inhomogeneouty of the poloidally averaged profiles seems to be quite natural because of a certain asymmetry of the outer and inner parts of the torus. Indeed, let us assume for a while that there exists longitudinally homogeneous poloidally averaged pressure profile in the SOL plasma, and that this profile is unstable against, say, RI-mode, otherwise there is no driving force for turbulent convection. This convection, in turn, causes deformation of the background pressure profile, namely, its flattening, within a time scale of about one-turn-over time of the conective cell, $\tau_\perp \sim \frac{l_\perp}{v_*}$ (here $l_\perp$ is the characteristic scale length of convective cell, and v_* is drift flow velocity in the cell; in the case of highly nonlinear flow this velocity is about a sound speed c_s). Then, in the toroidal geometry, the unfavourable curvature of the magnetic field lines, which is a driving force of the RI instability, is localized on the outside of the torus. Respectively, the growth of instability, accompanied by generation of convective cells, as well as the corresponding flattening of pressure profile, takes place outside of the torus only, while in the rest part of the SOL no driving force exists, and both the plasma convection and pressure profile flattening are considerably suppressed. Hence, the flattened background, i.e., poloidally averaged, pressure profile might be longitudinally inhomogeneous with the characteristic scale length of inhomogeneouty $l_\parallel$ of the order of the torus length. Usually $l_\parallel \gg l_\perp$, and the corresponding characteristic time scale of heavy ion longitudinal dynamics, $\tau_\parallel^{(i)} \sim \frac{l_\parallel}{c_s}$, is much larger than the convection time scale $\tau_\perp$, i.e, the longitudinal ion dynamics does not play essential role and can be neglected. As for inertialess electrons, they react immediately to any force disbalance along the field line and redistribute their density in such a way that the longitudinal force balance is recovered, mostly through the appearance of longitudinal electrostatic field. This process inevitably imposes the changes in poloidaly averaged profile of the electrostatic potential which, in turn, determines the poloidally averaged shear flow structure.

In the present paper, the described above mechanism of shear flow generation is considered in the simplest case of a slab SOL plasma geometry in the plane perpendicular to strong magnetic field, while the longitudinal plasma inhomogene-

outy and corresponding differential operators are treated in a "finite-difference" or "single-mode" approximation. This allows to consider still two-dimensional problem with taking into account some important features of three-dimensional plasma dynamics.

The paper is organized as follows. In section 2 basic equations are introduced and the model is described with some details. In section 3 the results of large scale numerical simulation are presented which clearly demonstrate the onset of ELM-like activity and shear flow generation. Two different regimes controlled by either interchange instability or Boltzman coupling are found and discussed. In section 4 low-dimensional model of the phenomenon is considered. The conclusions are summarized in section 5.

2. BASIC EQUATIONS

In many respects, dynamics of scrape-off-layer plasma is described by two-fluid magnetohydrodynamic equations which are the continuity and momentum equations for the electron (e) and ion (i) components:

$$\frac{\partial n_\alpha}{\partial t} + \nabla(n_\alpha \mathbf{v}^\alpha) = 0, \tag{1}$$

$$\frac{d\mathbf{v}^\alpha}{dt} = \frac{e_\alpha}{m_\alpha}(\mathbf{E} + \frac{1}{c}[\mathbf{v}^\alpha \times \mathbf{B}]) - \frac{1}{n_\alpha m_\alpha}\nabla P_\alpha + \frac{1}{\tau_{ei}}(\mathbf{v}^\beta - \mathbf{v}^\alpha) + \nu_\alpha \Delta \mathbf{v}^\alpha. \tag{2}$$

Here $\frac{d\mathbf{v}^\alpha}{dt} \equiv \frac{\partial \mathbf{v}^\alpha}{\partial t} + (\mathbf{v}^\alpha \cdot \nabla)\mathbf{v}^\alpha$; $\alpha = e, i$, $\beta = i, e$; n_α , $\mathbf{v}^\alpha$ and P_α are density, velocity and pressure of the α-th component, respectively; τ_{ei} is characteristic momentum exchange time between ions and electrons closely related with plasma electric resistivity; ν_α is the kinematic viscosity coefficient; other notations are as usual.

Drift convection, which we are interested in, is relatively slow process in comparison with plasma oscillations, and charge separation effects are averaged out on the convective time scale. In this case, with high accuracy, plasma is assumed to be quasineutral, $n_e = n_i = n$, although an electrostatic potential of the plasma, φ, is not necessarily equal to zero. Slow evolution of the electrostatic potential is described by the equation for electric charge density, $(n_i - n_e)$, with averaged out fast time derivative term,

$$\nabla \cdot \mathbf{J} = 0, \tag{3}$$

where $\mathbf{J} \equiv e(n_i \mathbf{v}_i - n_e \mathbf{v}_e)$ is an electric current density. In explicit form, the relationship between equation (3) and evolution of the electrostatic potential becomes clear when plasma dynamics, i.e., the velocity $\mathbf{v}^{e,i}$, is substituted explicitly (see equation (8)). Then, the electron continuity equation (1) can be considered as the equation for quasineutral plasma density n ,

$$\frac{\partial n}{\partial t} + \nabla_\perp(n\mathbf{v}_\perp) - \frac{1}{e}\nabla_\parallel J_\parallel = 0, \tag{4}$$

where "$\|$" and "$\perp$" stand for the directions along and across the magnetic field $\mathbf{B}$, respectively, i.e., for example, $\nabla_\| \equiv (\frac{\mathbf{B}}{B} \cdot \nabla)$, $\nabla_\perp \equiv \nabla - \frac{\mathbf{B}}{B}\nabla_\|$ and so on. Longitudinal part of the divergency $\nabla(n\mathbf{v})$ in equation (4) is expressed in terms of electron longitudinal velocity only, i.e., in terms of longitudinal electric current, $\nabla_\|(nv_\|) \approx -\frac{1}{e}(\nabla_\| J_\|)$, while the longitudinal dynamics of heavy ion is neglected.

In order to close the set (3) and (4) we have to express perpendicular flow velocity $\mathbf{v}_\perp$ and longitudinal current density $J_\|$ in terms of the principal variables n and φ.

Hereafter, we assume that the magnetic field perturbation is absent and, hence, only the potential electric field $\mathbf{E} = -\nabla_\perp\varphi$ should be taken into account in equation (2). Then, steady-state magnetic field in the SOL is as strong as this is in the bulk plasma. So, in the main order of B^{-1} expansion, the perpendicular flow velocity $\mathbf{v}_\perp$ corresponds to the $[\mathbf{E} \times \mathbf{B}]$-drif,

$$\mathbf{v}_\perp = \frac{c}{B^2}[\mathbf{E} \times \mathbf{B}] = \frac{c}{B^2}[\mathbf{B} \times \nabla_\perp\varphi] \tag{5}$$

Expression (5) follows from equation (2) with neglected pressure and inertia terms which, however, should be retained in equation (3) for the electrostatic potential (see below, equation (8)).

In the considered approximation, longitudinal component of electric current density is determined by longitudinal electron motion only and can be found from the momentum equation (2). For the inertialess electrons one obtains:

$$\frac{1}{\sigma}J_\| = -\nabla_\|\varphi + \frac{1}{en}\nabla_\| P_e, \tag{6}$$

where $\sigma^{-1} = \frac{m_e}{ne^2\tau_{ei}} = \frac{4\pi}{\tau_{ei}\omega_{pe}^2}$ is plasma resistivity. The momentum exchange time scale τ_{ei} is not specified in the present analysis, and it is sufficient to treat σ as a phenomenological plasma parameter ($\sigma = constant$). For the same reason, it is sufficient to assume that plasma temperature T is a constant as well. Then the longitudinal part of electric current divergency can be written as

$$(\nabla_\| J_\|) \approx \sigma\nabla_\|^2(-\varphi + \frac{T}{e}\ln(n)). \tag{7}$$

Thus, in low-resistive, $\sigma^{-1} \to 0$, longitudinally inhomogeneous, $\nabla_\| \neq 0$, plasma the longitudinal electron dynamics tends to establish Boltzman distribution with strongly coupled plasma density and electrostatic potential, $n \sim \exp(\frac{e\varphi}{T})$. Note that equation (7) and, hence, Boltzman coupling effect are valid for the poloidally averaged n and φ as well.

Substituting expression (7) into equation (3) and also using the general equality $(\nabla_\perp \cdot \mathbf{J}_\perp) \equiv \nabla_\perp\{\frac{1}{B^2}[\mathbf{B} \times [\mathbf{J}_\perp \times \mathbf{B}]]\}$ with the magnetic pondermotive force $[\mathbf{J}_\perp \times \mathbf{B}]$ taken from momentum equation (2), one obtains equation for plasma flow vorticity, $rot_\|\mathbf{v}_\perp \approx \frac{c}{B}\nabla_\perp^2\varphi$ (or, equivalently, for the electrostatic potential). Namely,

$$\frac{\partial \nabla_\perp^2 \varphi}{\partial t} + \frac{c}{B}[\nabla_\perp \varphi \times \nabla_\perp \nabla_\perp^2 \varphi]_\| - (\nu_\perp \nabla_\perp^2 + \nu_\| \nabla_\|^2)\nabla_\perp^2 \varphi =$$

$$= -\frac{TB^3}{m_i nc}[\nabla_\perp(\frac{1}{B^2}) \times \nabla_\perp n]_\| + \frac{\sigma B^2}{m_i nc^2}\nabla_\|^2(-\varphi + \frac{T}{e}\ln(n)). \qquad (8)$$

Here we neglect all the plasma inhomogeneouty and inertia effects retaining only the most important ones: i) convective and diffusive vorticity transport (see the left hand side of equation (8)), ii) an effective "gravitational" driving force in a curved magnetic field, $-\frac{TB^3}{m_i nc}[\nabla_\perp(\frac{1}{B^2}) \times \nabla_\perp n]_\|$, and iii) Boltzman coupling term in the r.h.s., respectively.

There exists analogy between interchange instability in magnetized plasma and Rayleigh-Taylor instability in stratified fluid. It is based on the analogy between magnetic curvature effect and gravity action. Indeed, in the case of Rayleigh-Taylor instability, flow evolution is described by Euler equation, $\frac{d\mathbf{v}}{dt} = -g\mathbf{e}_x - \frac{1}{\rho}\nabla P$, where g is the gravitational acceleration along, say, the x-direction, and ρ is spatially inhomogeneous mass density. Respectively, the flow vorticity, $rot\ \mathbf{v}$, is driven by the forcing term $\frac{\partial}{\partial t} rot\ \mathbf{v} \sim -[\nabla(\frac{1}{\rho}) \times \nabla P] \sim \frac{g}{\rho}[\mathbf{e}_x \times \nabla \rho]$ where it is assumed that, for slow fluid dynamics, pressure gradient is mainly determined by its hydrostatic quasi-equilibrium value, $\nabla P \approx -g\rho\mathbf{e}_x$. This gravitational driving force is obviously analogous to the magnetic curvature driving force in equation (8) with an effective "gravitational acceleration" $g \sim \frac{T}{m_i}\frac{|\nabla_\perp B|}{B} \sim \frac{c_s^2}{R}$ (here $R \sim l_\|$ is the tokamak major radius).

So far, we considered three-dimensional plasma dynamics. Let us now simplify the problem and reduce its dimensionality by representing the longitudinal differential operator $\nabla_\|^2$ in its "finite-difference" form: $\nabla_\|^2 \approx -l_\|^{-2}$. This, actually, corresponds to a single-mode approach with the only characteristic harmonic in the direction along the magnetic field. Such an approach is quite reasonable unless the detailes of nonlinear flow (or waves) propagation along the field lines come to light. In the present qualitative analysis we neglect any longitudinal plasma dynamics, besides Boltzman coupling effect, and consider only "robust" longitudinal inhomogeneouty in the form of a bump-like localization of the instability-driven convection mainly in the inner part of an open magnetic field line in the SOL, while outside the covection region, if seeing along the field line, there exist unperturbed (e.g., not flattened) background plasma density and potential profiles, n_b and φ_b , respectively. In the simplest case, we assume that no externally driven plasma flow exists in the SOL, i.e., $\varphi_b = 0$. Then, without loss of generality, we also assume that $|n - n_b| \ll n_b$ and, hence, $\nabla_\|^2 \ln(n) \sim -l_\|^{-2}\frac{(n-n_b)}{n_b}$. With such a simplifications, system (4) and (8) can be written in the following dimensionless form (see (17-26)):

$$\frac{\partial N}{\partial \tau} + [\nabla_\perp \Phi \times \nabla_\perp N]_Z + \frac{\partial \Phi}{\partial Y} - \sigma_2(\Phi - N) = D_\perp \nabla_\perp^2 N, \qquad (9)$$

$$\frac{\partial \nabla_\perp^2 \Phi}{\partial \tau} + [\nabla_\perp \Phi \times \nabla_\perp \nabla_\perp^2 \Phi]_Z + g_B \frac{\partial N}{\partial Y} - \sigma_1 (\Phi - N) = \mu_\perp \nabla_\perp^4 \Phi. \qquad (10)$$

Here $\Phi \equiv \frac{e\varphi}{T}$, $N \equiv \frac{(n - n_b)}{n_{b0}}$, n_{b0} and $(\frac{dn_b}{dx})_0$ are the characteristic density and radial density gradient of the background SOL plasma, $n_b \approx n_{b0}(1 + \frac{x}{n_{b0}}(\frac{dn_b}{dx})_0)$ Then, x, y and z are the Cortesian coordinates which correspond locally to radial, poloidal and toroidal directions, respectively. Dimensionless coordinates in the perpendicular ($\perp$) plane are $X \equiv \frac{x}{x_0}$ and $Y \equiv \frac{y}{x_0}$, where $x_0 \approx n_{b0} \mid (\frac{dn_b}{dx})_0 \mid^{-1}$ is the SOL width. Dimensionless time $\tau \equiv \frac{t}{t_0}$ is normalized by an effective Bohm diffusion time scale $t_0 = x_0^2 (\frac{cT}{eB})^{-1}$. In these notations, shear flow component corresponds to poloidally averaged poloidal velocity, $< v_Y > \equiv \frac{\partial < \Phi >}{\partial X}$, where $< \cdot > \equiv \frac{1}{Y_0} \int_0^{Y_0} (\cdot) dY$ represents poloidally averaged quantity.

In system (9) and (10), there are five dimensionless parameters though only three of them, actually, control the regime of flow evolution. Namely, parameter $g_B = 2\frac{x_0}{R}(\frac{x_0}{\rho_s})^2$, where $\rho_s = c_s(\frac{m_i c}{eB})$ is the ion Larmor radius, represents magnetic curvature effect and determines the growth rate of an ideal interchange, or Rayleigh-Taylor, instability, $\gamma_{RT} \approx \sqrt{g_B}$. Parameter $\sigma_1 = \sqrt{\frac{m_i}{m_e}} \frac{\lambda_{ei} x_0^4}{\rho_s^3 l_\parallel^2}$ controls the coupling between interchange and drift waves ($\lambda_{ei} = \tau_{ei}\sqrt{\frac{T}{m_e}}$ is the electron mean free path which determines plasma resistivity along the magnetic field). For perturbation with sufficiently large wave number, $k \gg (\frac{\sigma_1}{4})^{\frac{1}{3}}$, parameter σ_1 determines characteristic time scale of a particular type of drift instability, $\tau_\sigma \approx \sqrt{\frac{2k^2}{k_Y \sigma_1}}$. This follows from the expression for instability growth rate obtained from linearized equations (9) and (10),

$$\gamma \approx -k^2 D - \frac{\sigma_1}{2k^2} + Re\sqrt{\frac{\sigma_1^2}{4k^2} + g_B \frac{k_Y^2}{k^2} - i\frac{\sigma_1 k_Y}{k^2}}, \qquad (11)$$

where we neglect σ_2, for simplicity. The third control parameter, which is rather phenomenological one, is the diffusivity $D \approx D_\perp \approx \mu_\perp$. We assume that it is small but finite, in order to suppress small scale length perturbations with $k > k_*$, where k_* is a characteristic "cut-off" wave number. In the case when Boltzman coupling effect dominates, i.e., for $\tau_\sigma \gamma_{RT} \ll 1$, this wave number is $k_* \sim (\frac{\sigma_1}{2D^2}\frac{k_Y}{k})^{\frac{1}{5}}$, while in the opposite case of $\tau_\sigma \gamma_{RT} \gg 1$ it is $k_* \approx \sqrt{\frac{\gamma_{RT}}{D}}$. As this is also shown below,

the diffusivity D controls slow relaxation of stable shear flow structure towards the instability threshold and, thus, determines the period of ELM-like flow evolution. Other coupling parameter, $\sigma_2 \equiv \sigma_1(\frac{\rho_s}{x_0})^2$, is relatively small (this is because the ion Larmor radius is small) and does not play essential role until finite Larmor radius effect, i.e., the transition to Hasegawa-Mima equation, is considered.

In a hidden form, system (9) and (10) is also characterized by important geometrical parameter, namely, the aspect ratio of the SOL, which is equal to dimensionless length of the SOL in the poloidal direction, Y_0 . Usually, the SOL width x_0 is about 1 cm while tokamak minor radius is about 0.5 m, so that the aspect ratio is expected to be more than one hundred. However, for qualitative analysis, it is sufficient to consider its rather moderate value, say, $Y_0 = 5$, in order to model self-consistent nonlinear dynamics of a long chain of instability-driven vortices with about ten convective cells per the period Y_0.

Thus, in the present paper, we consider the following range of the parameter values: $g_B = 0 - 10^2$, $\sigma_1 = 0 - 10^3$, $D = 10^{-4} - 10^{-3}$ and $\sigma_2 = (10^{-4} - 10^{-2})\sigma_1$, which, hence, includes both the limiting cases of strong and weak Boltzman coupling effect. Relatively small diffusivity value is chosen in such a way when it allows the development of about ten Bénard-like convective cells per one poloidal period Y_0.

With such a parameters, governing equations (9) and (10) have been solved numerically. The simulation domain ($0 \leq X \leq 1$; $0 \leq Y \leq 5$) was implemented on a 101×501 grid point, respectively. As the boundary condition, we assumed periodicity along the poloidal Y-direction with the period $Y_0 = 5$, and the free-slip ($\nabla_\perp^2 \Phi \mid_{X=0;1} = 0$) condition at the rigid wall, where it was also suggested that $\Phi \mid_{X=0;1} = N \mid_{X=0;1} = 0$. The initial small amplitude (less than 10^{-6}) random perturbation of plasma density was considered, while the initial electrostatic potential was not perturbed at all, $\Phi \mid_{\tau=0} \equiv 0$.

3. SIMULATION RESULTS

Numerical simulation clearly demonstrates that, in all the cases within the considered parameter range, large shear flow component with the poloidal velocity $< v_Y > \sim 1$ is always generated, but its temporal evolution strongly depends on the coupling parameter value.

Let us consider, for the begining, typical flow evolution in the case when Boltzman coupling effect dominates, i.e., when $\tau_\sigma \gamma_{RT} \leq 1$ (namely, we consider the case of $\sigma_1 = 6$, $g_B = 1$ and $D = 7 \cdot 10^{-4}$).

In Figure 1, few successive snapshots showing plasma density (a) and potential (b) contour lines, as well as radial profiles of the poloidally averaged plasma density (c) and poloidal velocity (d), are presented for the very first cycle of shear flow generation. For $\tau < 15$, linear growth of interchange instability is accompanied by the development of the most unstable mode with characteristic wave number $k \approx \frac{2}{3} k_* \approx 14$. Then, at the nonlinear stage, $15 < \tau < 20$, the instability-driven convection causes significant spatial redistribution of the poloidally averaged plasma density profile (namely, its flattening) with corresponding rearrangement of the electrostatic potential and, hence, flow velocity profiles. The flattening of

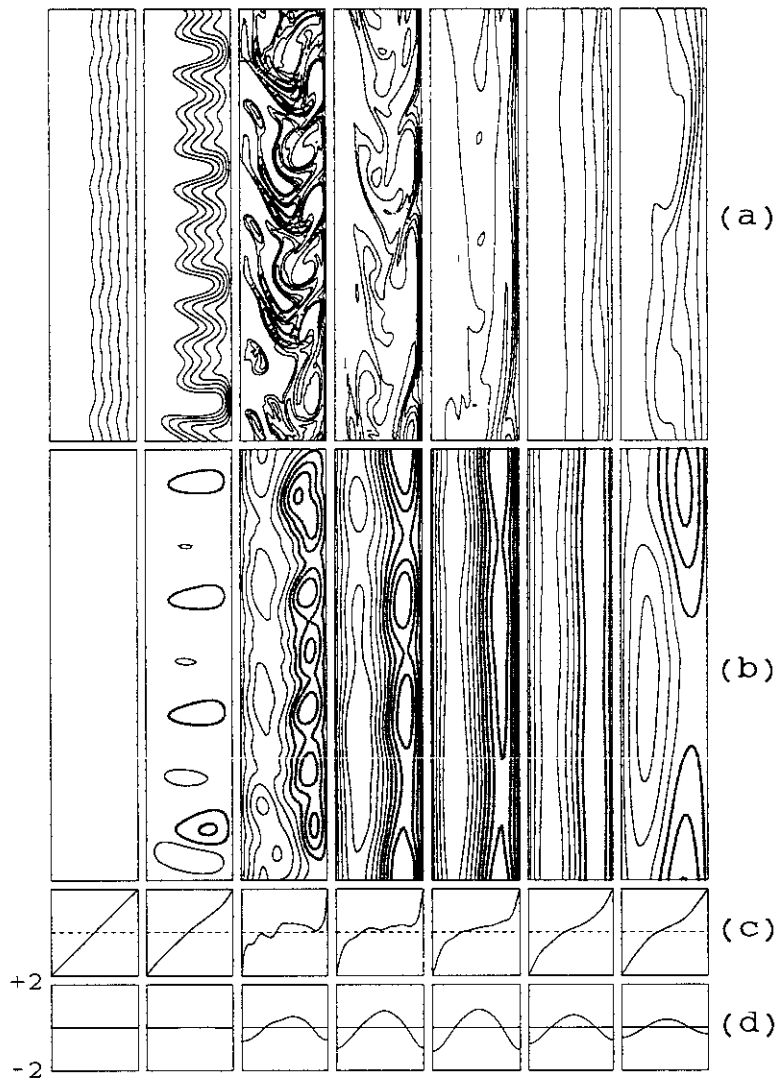

FIGURE 1. Snapshots of the contour lines for plasma density (a) and electrostatic potential (b) at the time moments $\tau = 11; 14; 17; 20; 24; 40; 60$ (from left to right) corresponding to the very first cycle of shear flow generation. Poloidally averaged profiles of plasma density (c) and poloidal flow velocity (d) are also shown (the case of $g_B = 1,\ \sigma_1 = 6$).

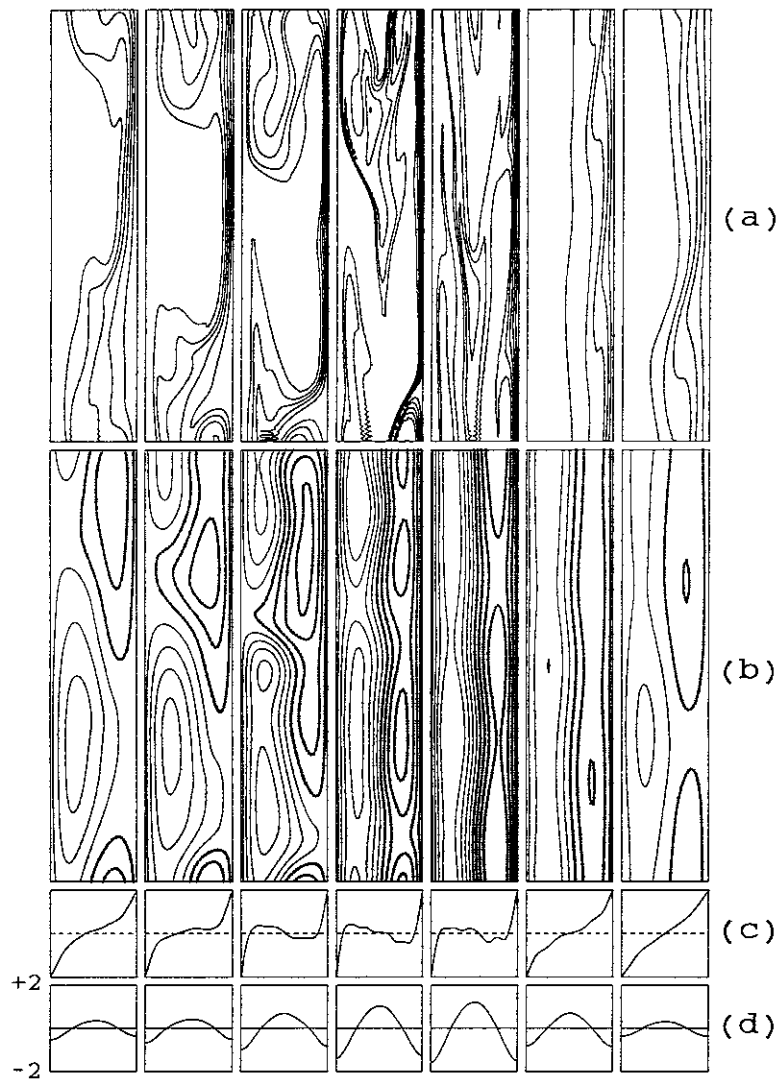

FIGURE 2. The same as in Figure 1 but for the second cycle of shear flow generation ($\tau = 62; 64; 66; 68; 70; 90; 116$, from left to right)

density profile and generation of large shear flow component, which stirs and suppresses the convective cells, also arrest the growth of instability. As a result, in the absence of free energy release, both the shear flow component and the perturbation of radial density profile slowly decay within relatively long period $\delta\tau$ of quiet evolution determined by plasma diffusivity. $\delta\tau \approx \frac{1}{D(2\pi)^2} \approx 35$, (see time interval $20 < \tau < 60$ in Fig.1). However, when the poloidal shear flow velocity becomes sufficiently small and spatial distribution of plasma density approaches its initial linear profile, the flow suffers another cycle of instability with the consequent generation of shear flow component (see Figure 2 which represents the second cycle of shear flow generation immediately successive to the first one given in Figure 1). Besides very initial period, $\tau < 15$, flow evolution during all the other successive cycles goes on in a similar periodical way and follows the same scenario described above. The only difference concerns the shape of unstable plasma density perturbation. For $\tau < 20$, Rayleigh-Taylor instability grows in the absence of any considerable shear flow component and is characterized by the development of narrow, radially elongated spikes of dense plasma. In contrast, plasma density perturbation during all the successive cycles of shear flow generation is usually of the form of poloidally elongated "bubble". When such a "bubble" approaches the wall (see, e.g., the time moment $\tau = 66$ in Fig.2). plasma density gradient and, hence, particle flux, $q = D\int_0^{Y_0}(1 - (\frac{\partial N}{\partial X})_{|X=0,1})\, dY$, grow there significantly. However, an efficient contact of the "bubble" with the wall takes place during a short period of time only, $\delta\tau < 10$, while during all the rest of a cycle the "bubble" is separated from the wall by shear flow separatrix, and the corresponding particle flux value is small. Respectively, time-averaged particle flux, $\bar{q} = \frac{1}{\tau_c}\int_\tau^{\tau+\tau_c} q\, d\tau$, is reduced and does not exceed considerably its value in the absence of turbulent convection. This is clearly seeing in Figure 3.a where time evolution of both the fluxes q and $\bar{q}$ is shown together with temporal behaviour of shear flow kinetic energy per unit length in the poloidal direction, $W_s \equiv \frac{1}{2}\int_0^1 (\frac{\partial < \Phi >}{\partial X})^2\, dX$.

In order to clarify the role played by Boltzman coupling effect in the observed strong correlation between the processes of plasma density flattening and shear flow generation, let us consider temporal evolution of shear flow kinetic energy, $\frac{dW_s}{d\tau} = P_R + P_B - Q$, and compare the driving terms which are the rate of Reynolds stresses, $P_R = -\int_0^1 \frac{\partial^2 < \Phi >}{\partial X^2} < \frac{\partial \Phi}{\partial X}\frac{\partial \Phi}{\partial Y} > dX$, the rate of Boltzman coupling, $P_B = -\sigma_1 \int_0^1 < \Phi > (< \Phi > - < N >)\, dX$, and dissipation rate, $Q = D\int_0^1 (\frac{\partial^2 < \Phi >}{\partial X^2})^2 dX$. Temporal evolution of these quantities is shown in Figure 3.b. One can easily see that Boltzman coupling effect always dominates over Reynolds stresses and, hence, plays important role in flow evolution. Then, during the phase of dissipative relaxation, the coupling rate P_B goes down much faster than the dissipative decay process as itself. This can be satisfactorily explained only by the establishment of Boltzman distribution, $< \Phi > \approx < N >$. Hence, Boltzman

coupling effect controls flow evolution during slow dissipative relaxation as well, eventhough, in this case, the dissipation rate Q formally exceeds the coupling rate P_B.

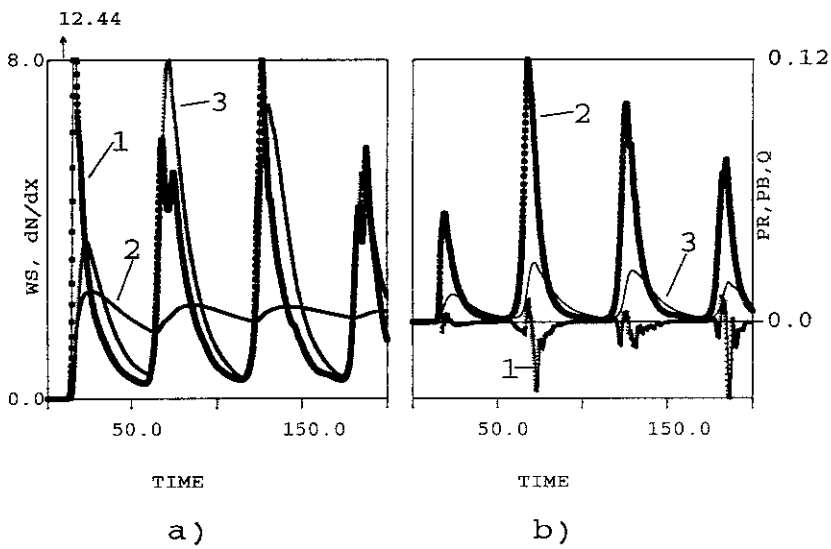

FIGURE 3.

(*a*) - ELM-like temporal evolution of the poloidally- (curve 1) and time-averaged (curve 2) density gradient at the wall, as well as the kinetic energy of shear flow component, W_s (curve 3);
(*b*) - shear flow energy balance: the rates of Reynolds stresses (curve 1), Boltzman coupling (curve 2) and dissipation (curve 3). The case of $g_B = 1$, $\sigma_1 = 6$.

In the opposite case of $\tau_\sigma \gamma_{RT} \geq 1$ (namely, for $g_B = 7$ with other parameters unchanged), magnetic curvature effect dominates, and flow evolution is changed considerably. First of all, this concerns generation of saturated poloidally averaged shear flow component. In contrast to the previous case, shear flow component, being initially generated within the period of two inverse ideal growth rates γ_{RT}, is then maintained at the same saturated level $< v_Y > \approx 1$ (see Fig.4, Fig.5 and Fig.6, which are the analogies of Fig.1, Fig.2 and Fig.3, respectively, but correspond to higher g_B value). The corresponding poloidally averaged density profile is flattened permanently as well. Hence, no considerable difference between the particle fluxes q and $\bar{q}$ appears (see Fig.6.a). Both the fluxes exceed at least twice

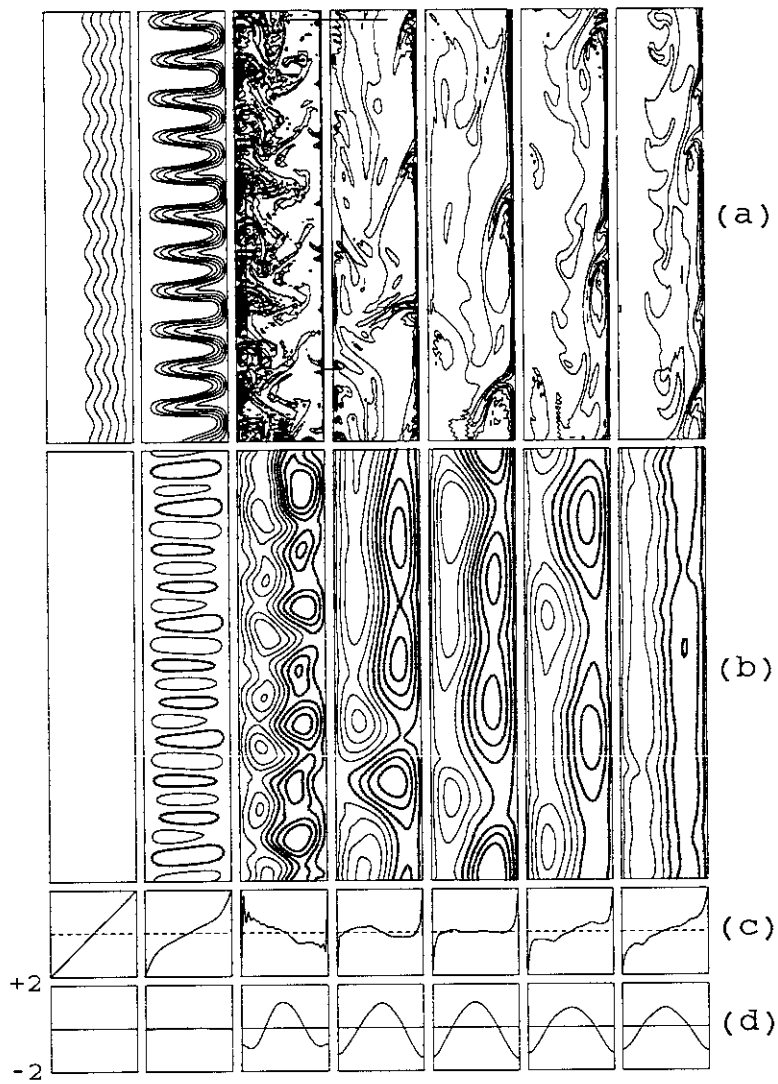

FIGURE 4. Snapshots of the contour lines for plasma density (a) and electrostatic potential (b) at the time moments $\tau = 4; 5; 6; 8; 10; 15; 20$ (from left to right) corresponding to the very first cycle of shear flow generation. Poloidally averaged profiles of plasma density (c) and poloidal flow velocity (d) are also shown (the case of $g_B = 7$, $\sigma_1 = 6$).

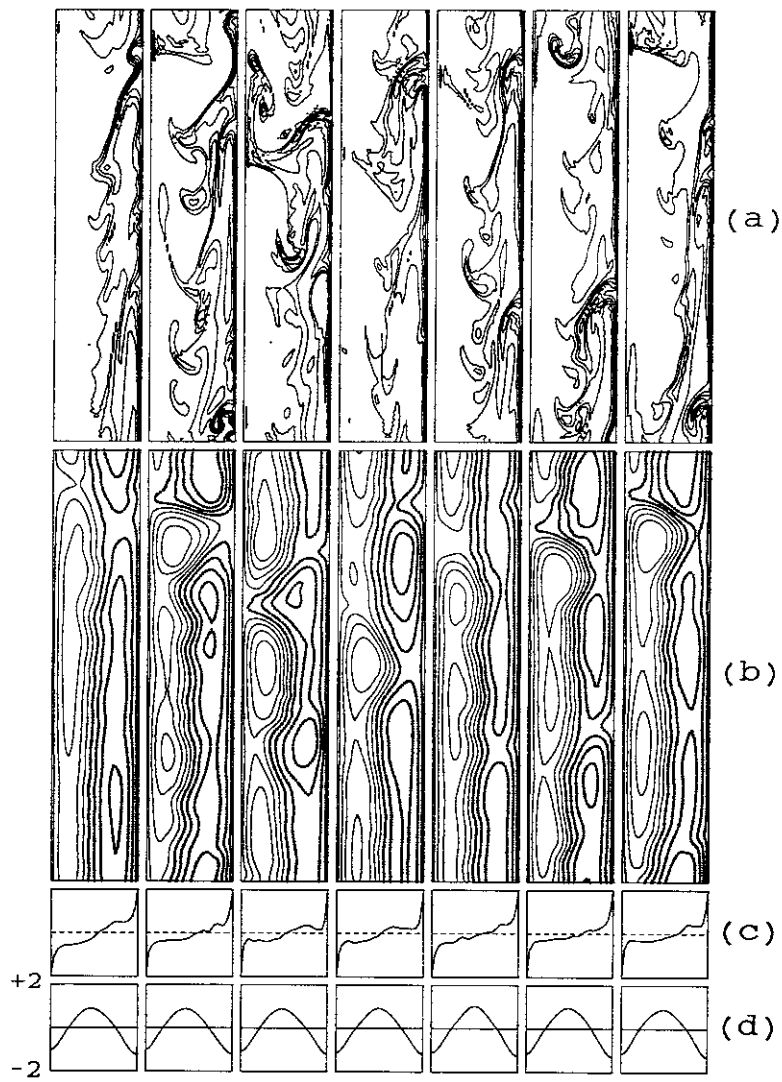

FIGURE 5. The same as in Figure 4 but for the time moments $\tau = 40; 42; 44; 46; 50; 56; 60$ (from left to right)

their values in the case of $\tau_\sigma \gamma_{RT} \leq 1$, what reminds degradation of plasma confinement in L-regime. However, an interesting feature of such a "strange" L-mode is the generation of steady-state shear flow component which, however, does not suppress interchange instability (this is because g_B is high enough) and co-exists with instability-driven Bénard-like convective cells (see Fig.6.b). As the vortices are strong, neither "spikes" nor "bubbles" are effectively separated from the walls by shear flow separatrix, and this explaines degradation of plasma confinement even in the presence of shear flow.

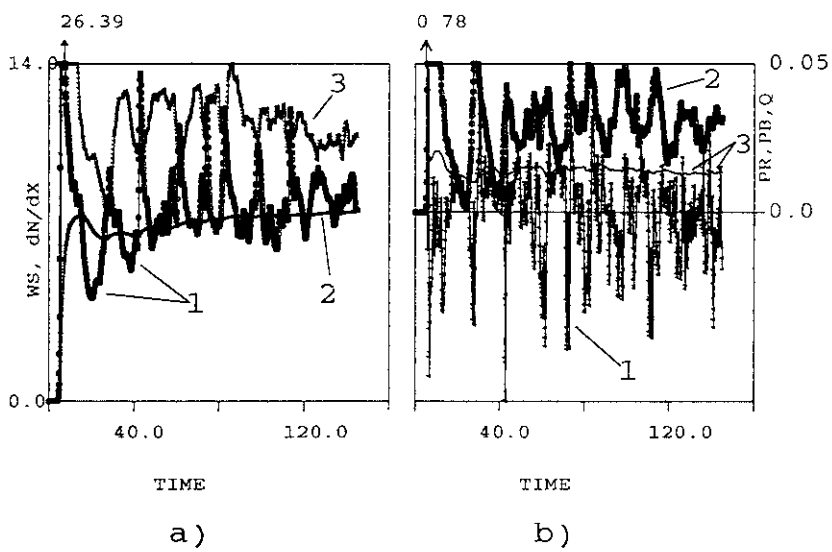

FIGURE 6. The same as in Figure 3 but for $g_B = 7$, $\sigma_1 = 6$.

In ($g_B - \sigma_1$)-plane, the described above two different regimes of plasma flow evolution , namely, ELMs and "strange" L-mode, are separated by the curve $\tau_\sigma \gamma_{RT} \sim 1$ or, equivalently, $\frac{g_B}{\sigma_1} \sim \frac{1}{2k}$ with the observed effective wave number of the "bubble" structure $k \sim 1$. Rather sharp transition from one regime to another takes place while moving across the separatrix. For example, the case $g_B = 5$, $\sigma_1 = 4$ corresponds to typical "strange" L-mode, while the case $g_B = 5$, $\sigma_1 = 6$ already corresponds to the ELM-like evolution, although with relatively short ELMs period, about 50 % of its typical value observed in the case of $g_B = 5$, $\sigma_1 = 10$.

4. LOW-DIMENSIONAL MODEL

The observed process of shear flow generation is, roughly speaking, a combination of four "robust" processes: i) density profile flattening via nonlinear convection; generation of shear component via ii) Boltzman coupling effect (when density profile is flattened) and/or iii) Reynolds stresses; and iv) slow dissipative relaxation of a stable configuration towards the instability threshold. These processes, according to the simulation results, seem to be irrelevant to the particular details of plasma density and potential spatial structure and, hence, their description in terms of low-dimensional model is quite reasonable. Such a model, if represents the process qualitatively well, could help in scanning wider range of plasma parameters and elucidate the physics of the phenomenon.

There exists well-known and successful example of such a low-dimensional model, namely, Lorentz set for Bénard convection in unstably stratified fluid. In Lorentz model (but in our notations), the only flow structure taken into account is a regular chain of vortices, $\Phi^{(L)} = b_\Phi^{(L)} \cos(k_Y Y) \sin(\pi X)$. As for density structure, it includes both profile flattening (the amplitude $A_N^{(L)}$) and a spike-like convective deformation (the amplitude $a_N^{(L)}$), so that $N^{(L)} = A_N^{(L)} \sin(2\pi X) + a_N^{(L)} \sin(k_Y Y) \sin(\pi X)$. This model describes well many features of Bénard convection, so it is meaningful to use the Lorentz set as a "kernel" of an extended low-dimensional model which takes into account the effect of shear flow generation (this effect is not included into the original Lorentz set).

One example of such an extended Lorentz model was considered in (18). However, Boltzman coupling effect did not play essential role in that simulation, and shear flow generation was mainly controled by Reynolds stresses forcing. Respectively, the density and potential structures considered in (18) did not represent intrinsically the coupling effect.

In the present paper we consider another type of an extended Lorentz set which is mainly oriented towards taking into account Boltzman coupling effect. In the original Lorentz set, density representation already includes both the important effects of profile flattening and spike- (or bubble)-like convective deformation, so it is quite reasonable to use the same density representation in our model as well. As for the representation of plasma potential, we have to explore the following observations (see the Figures presented above): i) poloidally averaged potential profile, $< \Phi >$, is always akin to density perturbation profile, and ii) there exists a tendency to establish Boltzman distribution, i.e., $(\Phi - N)$-coupling. This means that it is necessary (and, actually, sufficient) to include the density counterpart into the potential representation. With such a minimal correction, we consider the following density and potential structures:

$$N = A_N^{(L)} \sin(2\pi X) + a_N^{(L)} \sin(k_Y Y) \sin(\pi X),$$

$$\Phi = A_\Phi \sin(2\pi X) + [b_\Phi^{(L)} \cos(k_Y Y) + a_\Phi \sin(k_Y Y)] \sin(\pi X). \qquad (12)$$

Here (L) denotes an amplitude from the original Lorentz set. In the present analysis, characteristic poloidal wave number, $k_Y = \frac{2\pi m}{Y_0}$, where m is the corresponding poloidal mode number, is not specified self-consistently and should

be considered as a parameter. According to simulation results described above, poloidal mode number is about 10 at the very first cycle of shear flow generation, and it is reduced till $m = 1$ or $m = 2$ during all the successive cycles.

Substituting expressions (12) into the governing equations (9) and (10), we obtain the following extended Lorentz set:

$$\begin{aligned}
\frac{d\ A_N^{(L)}}{d\tau} &= -\lambda_1 A_N^{(L)} + \sigma_2 A_\Phi - \frac{m\pi^2}{Y_0}\ a_N^{(L)}\ b_\Phi^{(L)} \\
\frac{d\ a_N^{(L)}}{d\tau} &= -\lambda_2 a_N^{(L)} + \sigma_2 a_\Phi + \frac{2\pi m}{Y_0} b_\Phi^{(L)} + \pi\ A_N^{(L)}\ b_\Phi^{(L)} \\
\frac{d\ b_\Phi^{(L)}}{d\tau} &= -\lambda_3 b_\Phi^{(L)} + \gamma_B a_N^{(L)} + \xi\ A_\Phi\ a_\Phi \\
\frac{da_\Phi}{d\tau} &= -\lambda_4 a_\Phi + \gamma_\sigma a_N^{(L)} - \xi\ A_\Phi\ b_\Phi^{(L)} \\
\frac{d\ A_\Phi}{d\tau} &= -\lambda_5 A_\Phi + \frac{\sigma_1}{4\pi^2}\ A_N^{(L)}
\end{aligned} \tag{13}$$

Here $\lambda_1 = 4\pi^2 D + \sigma_2$, $\lambda_2 = k^2 D + \sigma_2$, $\lambda_3 = \lambda_4 = k^2 D + \frac{\sigma_1}{k^2}$, $\lambda_5 = 4\pi^2 D + \frac{\sigma_1}{4\pi^2}$, $\xi = \frac{\pi^2 m}{k^2 Y_0}((\frac{2\pi m}{Y_0})^2 - 3\pi^2)$, $\gamma_B = \frac{g_B}{k^2}\frac{2\pi m}{Y_0}$, $\gamma_\sigma = \frac{\sigma_1}{k^2}$, $k^2 = \pi^2 + (\frac{2\pi m}{Y_0})^2$.

Last equation in the set (13) describes dissipative relaxation towards Boltzman distribution for the poloidally averaged potential and density profiles. This is, actually, the process of shear flow generation in the presence of the flattened density profile (see Introduction). As this follows from the first and the last equations (13), both the shear flow component and the flattening perturbation of plasma density profile tend to zero because of dissipative relaxation with characteristic dissipative time scale λ_5^{-1}. However, there exists a "source"-term in the right-hand-side of the equation for $A_N^{(L)}$, namely, the term with $a_N^{(L)} b_\Phi^{(L)}$, which generates nonzero amplitudes $A_N^{(L)}$ and, hence, A_Φ. This "source"-term describes nonlinear convective flattening of plasma density profile because of the development of a chain of vortices (amplitude $b_\Phi^{(L)}$) with consequent spike-like deformation of density profile (amplitude $a_N^{(L)}$). In turn, convection is driven by the development of instability which can be saturated by two nonlinearities arising from deformations of the poloidally averaged density and potential profiles: i) change in effective density gradient, i.e., $b_\Phi^{(L)} A_N^{(L)}$ term in the second equation (13), and ii) stiring of the vortices by shear flow component, i.e., the nonlinear terms in the third and fourth equations (13). Complicated interaction of these effects leads to ELM-like temporal behaviour of all the amplitudes.

Numerical solution of the set (13) is in a good agreement with the solution of the original set (9) and (10). In principle, the described low-dimensional model could be useful in the analysis of ELM activity in a wide range of plasma parameters. However, such an analysis is beyond the scope of the present paper.

5. CONCLUSIONS

We have studied, by two-dimensional large-scale numerical simulation, the process of shear flow generation in the plasma which is unstable against the growth of flute-like interchange perturbations. Particular attention was drawn to the effect of density and electrostatic potential coupling in longitudinally inhomogeneous plasma. This effect is shown to play a significant role in the onset of shear flow component.

Two different limiting cases of shear flow generation and evolution are found, depending on the importance of Boltzman coupling effect and driving force of interchange instability (magnetic curvature effect). When the coupling effect dominates, flow evolution is akin to ELM-activity in the SOL plasma with unessential degradation of plasma confinement. In the opposite case, plasma transport is enhanced considerably, eventhough shear flow component still exists. Between such a "strange" L-mode of plasma confinement, on the one hand, and ELM-like regime, on the other hand, there are various "transitional" regimes characterized by different values of the frequency of ELM-like events. In the $(g_B - \sigma_1)$-plane, however, there exists rather sharp boundary between these two regimes qualitatively corresponding to the balance between Boltzman coupling effect and the interchange instability driving force.

Low-dimensional model of the process is proposed. The model is based on well-known Lorentz set for Bénard convection with new elements which take into account shear flow generation and Boltzman coupling effect.

ACKNOWLEDGEMENT

This work was performed by using the Advanced Computing System for Complexity Simulation at NIFS under the support of Grants-in-Aid of the Ministry of Education, Science, Sports and Culture in Japan (No. 08044109).

One of the authors (S.B.) expresses his gratitude to Professors R. L. Dewar and R. W. Griffiths (the Australian National University) for kind hospitality, excellent working conditions and fruitful discussions during the Research Workshop on 2D Turbulence in Plasmas and Fluids.

REFERENCES

1. Wagner F. et al., *Phys. Rev. Lett.* **49**, 1408 (1982)
2. Groebner R. J. et al., in *Proceeings of the 16th European Conference on Controlled Fusion and Plasma Physics*, Venice, 1989 (European Physical Society, Petit-Lancy, Switzerland, 1989), p.245
3. Burrell K. H. et al., *Plasma Phys. Controlled Fusion* **31**, 1649 (1989)
4. Doyle E. J. et al., in *Proceedings of the 18th European Conference on Controlled Fusion and Plasma Physics*, Berlin, 1991 (Vienna: IAEA), **1**, p.285
5. Zohm H. et al., *Nuclear Fusion* **32**, 489 (1992)
6. Kerner W. et al., *Bull. Am. Phys. Soc.* **36**, 2R13 3210 (1991)
7. Erckmann V. et al., *Phys. Rev. Lett.* **70**, 2086 (1993)
8. Wagner F. et al., *Plasma Phys. Controlled Fusion* **36**, A61 (1994)

9. Toi K. et al., *Plasma Phys. Controlled Fusion* **36**, A117 (1994)
10. Shats M. et al., *Phys. Rev. Lett.* **77**, 4190 (1996)
11. Sakai O., Yasaka Y., and Itatani R., *Phys. Rev. Lett.* **70**, 4071 (1993)
12. Drake J. F. et al., *Phys. Fluids* **B 4**, 488 (1992)
13. Finn J. M., Drake J. F., and Guzdar P. N., *Phys. Fluids* **B 4**, 2758 (1992)
14. Finn J. M., *Phys. Fluids* **B 5**, 415 (1993)
15. Niedermeyer H. et al., in *Proceedings of the 18th European Conference on Controlled Fusion and Plasma Physics*, Berlin 1991 (Vienna: IAEA) **1**, p.301
16. Endler E. et al., in *Proceedings of the 20th International Conference on Controlled Fusion and Plasma Physics*, Lisboa 1993 (Vienna: IAEA) **2**, p.583
17. Kukharkin N. N., Osipenko M. V., Pogutse O. P., and Gribkov V. M., in *Proceedings of the 14th IAEA Conference on Plasma Physics and Controlled Nuclear Fusion Research* Würzberg, 1992 (Vienna: IAEA) **2**, p.293
18. Pogutse O., Kerner W., Gribkov V., Bazdenkov S., and Osipenko M., *Plasma Phys. Control. Fusion* **36**, 1963 (1994)
19. Bazdenkov S., and Pogutse O., *JETP Lett.* **57**, 426 (1993)
20. Sugama H., and Horton W., *Phys. Plasmas* **1**, 345 (1994)
21. Takayama A., Wakatani M., and Sugama H., *Phys. Plasmas* **3**, 3 (1996)
22. Takayama A., and Wakatani M., *Plasma Phys. Control. Fusion* **38**, 1411 (1996)
23. Yagi M., Wakatani M., and Hasegawa A., *J. Phys. Soc. Japan* **56**, 973 (1987)
24. Carreras B. A., Garcia L., and Diamond P. H., *Phys. Fluids* **30**, 1388 (1987)
25. Sugama H., and Wakatani M., *J. Phys. Soc. Japan* **57**, 2010 (1988)
26. R. B. White, *Theory of Tokamaks* Amsterdam: North-Holland, 1989, sec.6.

Recent Issues of NIFS Series

NIFS-459 K Araki, J Mizushima and S. Yanase,
The Non-axisymmetric Instability of the Wide-Gap Spherical Couette Flow; Oct 1996

NIFS-460 Y Hamada, A. Fujisawa, H. Iguchi, A. Nishizawa and Y. Kawasumi,
A Tandem Parallel Plate Analyzer; Nov 1996

NIFS-461 Y Hamada, A. Nishizawa, Y. Kawasumi, A. Fujisawa, K. Narihara, K. Ida, A. Ejiri, S. Ohdachi, K Kawahata, K. Toi, K. Sato, T. Seki, H. Iguchi, K. Adachi, S. Hidekuma, S.Hirokura, K. Iwasaki, T. Ido, M. Kojima, J. Koong, R. Kumazawa, H. Kuramoto, T. Minami, I. Nomura, H. Sakakita, M. Sasao, K.N. Sato, T. Tsuzuki, J. Xu, I. Yamada and T. Watari,
Density Fluctuation in JIPP T-IIU Tokamak Plasmas Measured by a Heavy Ion Beam Probe; Nov. 1996

NIFS-462 N. Katsuragawa, H. Hojo and A. Mase,
Simulation Study on Cross Polarization Scattering of Ultrashort-Pulse Electromagnetic Waves; Nov. 1996

NIFS-463 V. Voitsenya, V. Konovalov, O. Motojima, K. Narihara, M. Becker and B. Schunke,
Evaluations of Different Metals for Manufacturing Mirrors of Thomson Scattering System for the LHD Divertor Plasma; Nov. 1996

NIFS-464 M. Pereyaslavets, M. Sato, T. Shimozuma, Y. Takita, H. Idei, S. Kubo, K. Ohkubo and K. Hayashi,
Development and Simulation of RF Components for High Power Millimeter Wave Gyrotrons; Nov. 1996

NIFS-465 V.S. Voitsenya, S. Masuzaki, O. Motojima, N. Noda and N. Ohyabu,
On the Use of CX Atom Analyzer for Study Characteristics of Ion Component in a LHD Divertor Plasma; Dec. 1996

NIFS-466 H. Miura and S. Kida,
Identification of Tubular Vortices in Complex Flows; Dec. 1996

NIFS-467 Y. Takeiri, Y. Oka, M. Osakabe, K. Tsumori, O. Kaneko, T. Takanashi, E. Asano, T. Kawamoto, R. Akiyama and T. Kuroda,
Suppression of Accelerated Electrons in a High-current Large Negative Ion Source; Dec. 1996

NIFS-468 A. Sagara, Y. Hasegawa, K. Tsuzuki, N. Inoue, H. Suzuki, T. Morisaki, N. Noda, O. Motojima, S. Okamura, K. Matsuoka, R. Akiyama, K. Ida, H. Idei, K. Iwasaki, S. Kubo, T. Minami, S Morita, K. Narihara, T. Ozaki, K. Sato, C. Takahashi, K. Tanaka, K. Toi and I. Yamada,
Real Time Boronization Experiments in CHS and Scaling for LHD; Dec. 1996

NIFS-469 V.L. Vdovin, T.Watari and A. Fukuyama,

3D Maxwell-Vlasov Boundary Value Problem Solution in Stellarator Geometry in Ion Cyclotron Frequency Range (final report); Dec. 1996

NIFS-470 N. Nakajima. M. Yokoyama, M. Okamoto and J. Nührenberg,
Optimization of M=2 Stellarator; Dec. 1996

NIFS-471 A. Fujisawa, H. Iguchi. S. Lee and Y. Hamada,
Effects of Horizontal Injection Angle Displacements on Energy Measurements with Parallel Plate Energy Analyzer; Dec. 1996

NIFS-472 R. Kanno. N. Nakajima. H. Sugama, M. Okamoto and Y. Ogawa.
Effects of Finite-β and Radial Electric Fields on Neoclassical Transport in the Large Helical Device; Jan. 1997

NIFS-473 S. Murakami. N. Nakajima, U. Gasparino and M. Okamoto,
Simulation Study of Radial Electric Field in CHS and LHD; Jan. 1997

NIFS-474 K. Ohkubo. S. Kubo, H Idei, M. Sato. T. Shimozuma and Y. Takita,
Coupling of Tilting Gaussian Beam with Hybrid Mode in the Corrugated Waveguide; Jan. 1997

NIFS-475 A. Fujisawa. H. Iguchi. S. Lee and Y. Hamada,
Consideration of Fluctuation in Secondary Beam Intensity of Heavy Ion Beam Prove Measurements; Jan. 1997

NIFS-476 Y. Takeiri, M. Osakabe. Y. Oka, K. Tsumori, O. Kaneko, T. Takanashi, E. Asano, T. Kawamoto. R. Akiyama and T. Kuroda,
Long-pulse Operation of a Cesium-Seeded High-Current Large Negative Ion Source; Jan. 1997

NIFS-477 H. Kuramoto, K. Toi, N. Haraki, K. Sato, J. Xu, A. Ejiri, K. Narihara, T. Seki, S. Ohdachi, K. Adati. R. Akiyama, Y. Hamada, S. Hirokura, K. Kawahata and M. Kojima,
Study of Toroidal Current Penetration during Current Ramp in JIPP T-IIU with Fast Response Zeeman Polarimeter; Jan., 1997

NIFS-478 H. Sugama and W. Horton,
Neoclassical Electron and Ion Transport in Toroidally Rotating Plasmas; Jan. 1997

NIFS-479 V.L. Vdovin and I.V. Kamenskij,
3D Electromagnetic Theory of ICRF Multi Port Multi Loop Antenna; Jan. 1997

NIFS-480 W.X. Wang, M. Okamoto, N. Nakajima, S Murakami and N. Ohyabu,
Cooling Effect of Secondary Electrons in the High Temperature Divertor Operation; Feb. 1997

NIFS-481 K. Itoh. S.-I. Itoh. H. Soltwisch and H.R. Koslowski,
Generation of Toroidal Current Sheet at Sawtooth Crash; Feb. 1997

NIFS-482 K. Ichiguchi,
Collisionality Dependence of Mercier Stability in LHD Equilibria with Bootstrap Currents; Feb. 1997

NIFS-483 S. Fujiwara and T. Sato,
Molecular Dynamics Simulations of Structural Formation of a Single Polymer Chain: Bond-orientational Order and Conformational Defects; Feb. 1997

NIFS-484 T. Ohkawa,
Reduction of Turbulence by Sheared Toroidal Flow on a Flux Surface; Feb. 1997

NIFS-485 K. Narihara, K. Toi, Y. Hamada, K. Yamauchi, K. Adachi, I. Yamada, K. N. Sato, K. Kawahata, A. Nishizawa, S. Ohdachi, K. Sato, T. Seki, T. Watari, J. Xu, A. Ejiri, S. Hirokura, K. Ida, Y. Kawasumi, M. Kojima, H. Sakakita, T. Ido, K. Kitachi, J. Koog and H. Kuramoto,
Observation of Dusts by Laser Scattering Method in theJIPPT-IIU Tokamak Mar. 1997

NIFS-486 S. Bazdenkov, T. Sato and The Complexity Simulation Group,
Topological Transformations in Isolated Straight Magnetic Flux Tube; Mar. 1997

NIFS-487 M. Okamoto,
Configuration Studies of LHD Plasmas; Mar. 1997

NIFS-488 A. Fujisawa, H. Iguchi, H. Sanuki, K. Itoh, S. Lee, Y. Hamada, S. Kubo, H. Idei, R. Akiyama, K. Tanaka, T. Minami, K. Ida, S. Nishimura, S. Morita, M. Kojima, S. Hidekuma, S.-I. Itoh, C. Takahashi, N. Inoue, H. Suzuki, S. Okamura and K. Matsuoka,
Dynamic Behavior of Potential in the Plasma Core of the CHS Heliotron/Torsatron; Apr. 1997

NIFS-489 T. Ohkawa,
Pfirsch - Schlüter Diffusion with Anisotropic and Nonuniform Superthermal Ion Pressure; Apr. 1997

NIFS-490 S. Ishiguro and The Complexity Simulation Group,
Formation of Wave-front Pattern Accompanied by Current-driven Electrostatic Ion-cyclotron Instabilities; Apr. 1997

NIFS-491 A. Ejiri, K. Shinohara and K. Kawahata,
An Algorithm to Remove Fringe Jumps and its Application to Microwave Reflectometry; Apr. 1997

NIFS-492 K. Ichiguchi, N. Nakajima, M. Okamoto,
Bootstrap Current in the Large Helical Device with Unbalanced Helical Coil Currents; Apr. 1997

NIFS-493 S. Ishiguro. T Sato, H. Takamaru and The Complexity Simulation Group,
V-shaped dc Potential Structure Caused by Current-driven Electrostatic Ion-cyclotron Instability; May 1997

NIFS-494 K. Nishimura, R. Horiuchi, T. Sato,
Tilt Stabilization by Energetic Ions Crossing Magnetic Separatrix in Field-Reversed Configuration; June 1997

NIFS-495 T. -H Watanabe and T. Sato,
Magnetohydrodynamic Approach to the Feedback Instability; July 1997

NIFS-496 K. Itoh T Ohkawa. S. -I.Itoh, M. Yagi and A. Fukuyama
Suppression of Plasma Turbulence by Asymmetric Superthermal Ions; July 1997

NIFS-497 T. Takahashi, Y. Tomita. H. Momota and Nikita V. Shabrov,
Collisionless Pitch Angle Scattering of Plasma Ions at the Edge Region of an FRC, July 1997

NIFS-498 M. Tanaka. A.Yu Grosberg. V.S. Pande and T. Tanaka,
Molecular Dynamics and Structure Organization in Strongly-Coupled Chain of Charged Particles; July 1997

NIFS-499 S. Goto and S. Kida,
Direct-interaction Approximation and Reynolds-number Reversed Expansion for a Dynamical System; July 1997

NIFS-500 K. Tsuzuki, N. Inoue, A. Sagara, N. Noda, O. Motojima, T. Mochizuki, T. Hino and T. Yamashina,
Dynamic Behavior of Hydrogen Atoms with a Boronized Wall; July 1997

NIFS-501 I. Viniar and S. Sudo.
Multibarrel Repetitive Injector with a Porous Pellet Formation Unit; July 1997

NIFS-502 V. Vdovin. T. Watari and A. Fukuyama,
An Option of ICRF Ion Heating Scenario in Large Helical Device; July 1997

NIFS-503 E. Segre and S. Kida,
Late States of Incompressible 2D Decaying Vorticity Fields; Aug. 1997

NIFS-504 S. Fujiwara and T. Sato,
Molecular Dynamics Simulation of Structural Formation of Short Polymer Chains; Aug. 1997

NIFS-505 S. Bazdenkov and T. Sato
Low-Dimensional Model of Resistive Interchange Convection in Magnetized Plasmas; Sep. 1997